Heats of Transfer in the Diffusion Layer before the Surface and the Surface Temperature for a Catalytic Hydrogen Oxidation ($H_2 + (1/2)O_2 \rightarrow H_2O$) Reaction

Lianjie Zhu, Ger J. M. Koper,* and Dick Bedeaux†

DelftChemTech, Delft University of Technology, Julianalaan 136, 2628 BL Delft, The Netherlands, and Department of Chemistry, Norwegian University of Science and Technology, 7491 Trondheim, Norway

Received: November 1, 2005

The surface temperature and surface mole fractions are calculated for a catalytic hydrogen oxidation reaction over a Pt/Al_2O_3 catalyst pellet. The thermodynamics of irreversible processes was used in order to ensure the correct introduction of coupled heat and mass transfer. Two pathways, one using the 4×4 resistivity matrix and the other using a simplified effective conductivity matrix, were proven to yield equivalent results. By using expressions for the thermal diffusion coefficients, heats of transfer, and the Maxwell−Stefan diffusion coefficients given in the literature, available experimental data could be reproduced. The Dufour effect was found to be negligible for the prediction of the surface temperature. Neglecting the Soret effect would increase the predicted value of the surface temperature significantly—more than 30 K out of an average of about 400 K. It is found that the reaction rate can be used to predict the surface temperature.

1. Introduction

The diffusion thermoeffect or Dufour effect is the heat flux caused by a chemical potential gradient. The Dufour effect is usually significant for gaseous systems as has, for instance, been discussed by Sawford et al.[1] and more recently by Hort et al.[2] A very interesting phenomenon was described by Linz,[3] who found significant temperature variations in binary gas mixtures when a time-dependent external concentration gradient was applied. The reciprocal process, thermal diffusion or the Soret effect, is the diffusional flux induced by a temperature gradient. In several studies,[1,4,5] it was found that the Dufour effect can induce a temperature difference up to 4 K depending on the initial composition and pressure. Convection can be induced by a large Soret effect.[6−8] In a chemical vapor deposition reactor, the deposition rate was found to be changed up to 20% because of the Soret effect for some systems,[9] while it was negligible for other systems.[10] In solid−gas catalytic systems, both the Dufour effect and the Soret effect will generally be important because of the significant concentration and temperature gradients between the surface and the gas bulk phase due to the surface reaction. As we shall demonstrate, neglecting the Dufour and Soret effects may lead to erroneous predictions for the surface reaction rate, the driving forces for heat and mass transport, and the surface temperature. Since the surface temperature is the temperature at which the catalyzed reaction takes place and because this temperature is not easily measured, accurate predictions are needed to compare with the experimental determinations and for subsequent kinetics studies.

A systematic method of combining heat and mass transfer is provided by the thermodynamics of irreversible processes (TIP).[11] In this method, the heat and mass fluxes are linearly related to the thermodynamic forces, i.e., the temperature and chemical potential gradients, in the system. In particular, this method allows for a systematic study of the influence of the Dufour and Soret effects for various situations. The diagonal elements in the coefficient matrix are related to the well-known Fourier and Fick processes, whereas the nondiagonal elements represent cross-effects such as the Dufour and Soret effects.

In the present paper, we demonstrate the use of TIP on a catalytic hydrogen oxidation reaction ($H_2 + (1/2)O_2 \rightarrow H_2O$) in the steady state using experimental information available for this system. The system of choice consists of a single catalyst pellet as has been extensively studied by Maymo et al.[12] In the experimental conditions of this system, the gas outside the film closely approaches ideal stirred-tank conditions with known gas concentrations and temperature. The catalyst surface temperature as well as the oxygen surface concentration were given in ref 12. This is sufficient information to compute the remaining two surface concentrations, because in the steady state, the fluxes are related by stoichiometry.

The film model, as sketched in Figure 1, is used to analyze this system. The temperature and concentration gradients are assumed only to exist in a thin film around the catalyst pellet. The thickness of the film is δ. We deviate from the conditions in the experiment by assuming good conduction at the surface of the pellet so that the surface temperature and the pellet temperature are equal to the gas film temperature near the surface. This implies that we focus on the temperature difference across the gas film and do not consider the temperature difference between the surface and the center of the pellet. This is sufficient to assess the importance of the Dufour and Soret effects. Two alternative methods are used to relate the fluxes through and the thermodynamic forces across the thin film. The first method expresses the differences in temperature and chemical potentials across the film in terms of the fluxes using resistivity coefficients

$$\begin{cases} \Delta\left(\dfrac{1}{T}\right) = r_{qq}J'_q + \displaystyle\sum_{i=1}^{n} r_{qi}J_i \\ -\dfrac{\Delta\mu_{i,T}}{T} = r_{iq}J'_q + \displaystyle\sum_{j=1}^{n} r_{ij}J_j \end{cases} \tag{1}$$

Here, J'_q is the measurable heat flux and J_i the molar flux of

* Corresponding author. Email: g.j.m.koper@tudelft.nl.
† Norwegian University of Science and Technology.

10.1021/jp056301i CCC: $33.50
Published on Web 03/02/2006

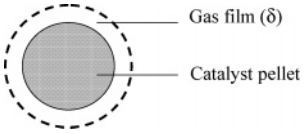

Figure 1. Schematic diagram of a catalyst pellet and the gas film at the external surface.

component *i*. Component *i* represents H_2, O_2, and H_2O, respectively. The resistivities include the film thickness and are subject to Onsager symmetry. Furthermore, μ_i is the chemical potential of the component *i*, and the subscript *T* signifies that the gradient is evaluated at constant temperature. The direction of the heat and mass transport is normal to the catalyst surface. The second method expresses the fluxes in terms of the temperature and chemical potential differences across the film using conductivity coefficients. This method allows for an approximation where the six independent mass transfer conductivities are simplified into three effective conductivities $l_{i,\mathrm{eff}}$.

$$\begin{cases} J'_q = l_{qq}\Delta\left(\frac{1}{T}\right) - \frac{1}{T}\sum_i l_{qi}\Delta\mu_{i,T} \\ J_i = l_{qi}\Delta\left(\frac{1}{T}\right) - \frac{1}{T} l_{i,\mathrm{eff}}\,\Delta\mu_{i,T} \end{cases} \tag{2}$$

In this film model, we combine heat and mass transfer, and only one film thickness will be used even though usually the film thickness is assumed to be different for heat and for mass transport. In the discussion of the results, we shall come back to this issue. The Dufour and Soret effects are contained within the cross-coefficients r_{qi} and l_{qi} that both can be expressed in terms of the heats of transfer. Many methods are presented in the literature[13−20] to measure or predict the heat of transfer in liquid solutions, solids, liquid−vapor interfaces, and so forth. Here, the expression for the heat of transfer analogous to the one by Taylor and Krishna for the continuous case is used;[21] see also ref 11. The boundary conditions for the above eqs 1 and 2 are twofold. On the pellet side, the mass fluxes are related by the chemical reaction rate and the mass balance. The reaction heat is carried away by the heat flux. No reaction is taking place in the film; hence, the fluxes are constant all through the film. On the other side, the gas concentrations and temperature are fixed by those in the gas phase.

To be able to predict the temperature and concentrations at the surface, the coefficients in the above eqs 1 and 2 need to be determined. In section 2, we shall first compute the heats of transfer for the various components and study their composition and temperature dependence. Subsequently, the resistivity coefficients are determined in section 3, and the catalyst surface temperature and concentrations close to the surface are calculated and compared with experimental data. The influence of the Dufour and Soret effects are investigated as well in these sections. The results demonstrate that the surface temperature is strongly influenced by the Soret effect and not so much by the Dufour effect as intuitively might be expected.[22−24] In section 4, we calculate the effective conductivity coefficients and confirm the results of section 3.

2. Heats of Transfer

Both the Dufour and Soret effects involve the heats of transfer Q_i^*. Values for this quantity cannot be found in the literature for the particular reaction at hand. We use a relation in terms of the thermal diffusion coefficients D_i^{T} given by Taylor and Krishna[21]

$$Q_i^* = \sum_{\substack{j=1 \\ j\neq i}}^{n} \frac{x_j RT}{D_{ij}}\left(\frac{D_i^{\mathrm{T}}}{\rho_i} - \frac{D_j^{\mathrm{T}}}{\rho_j}\right) \tag{3}$$

In the Appendix, two methods are given to obtain this expression. In these two methods, the heats of transfer are derived as being the ratio of two resistivity or conductivity coefficients; see refs 11 and 25. Unfortunately, the thermal diffusion coefficients are usually provided in units of mass per meter second so that we need to divide by the mass densities ρ_i. Furthermore, x_i represents the mole fraction of component *i*, *R* is the gas constant, and D_{ij} represents the Maxwell Stefan diffusion coefficients. Using Galilean invariance, it follows from eq 33 in the Appendix that the heats of transfer obey the following relation

$$\sum_i c_i Q_i^* = 0 \tag{4}$$

where c_i are molar concentrations. This relation can be used as a test on the obtained values of Q_i^*. Equation 3 satisfies this relation.

The concentration dependence of the heats of transfer is first investigated. The conditions for the calculations are taken from the experiment by Maymo et al., which are at 1 atm pressure and a temperature of 415 K. The mole fraction of water is 0.023, and the mole fractions for hydrogen and oxygen are in the ranges 0.966−0.772 and 0.011−0.205, respectively. The Maxwell−Stefan diffusion coefficients are calculated using eq 47 (see the Appendix) where the molecular mass M_i, the diameter d_i, and the thermal conductivity λ_i for the components H_2, O_2, and H_2O are given in Table 1. The thermal diffusion coefficients are evaluated using a computer program by Kleijn and Dorsman[26] based on Hirschfelder's method.[27] Subsequently, the heats of transfer are calculated using eq 3 for various mole fractions of the gases. The results demonstrate that oxygen transfers the largest amount of heat per mole among these three gases. Therefore, the heats of transfer of the three gases are calculated keeping the mole fraction of water vapor constant and varying the mole fractions of oxygen and hydrogen. Since the thermal diffusion coefficient is an important parameter for the heat of transfer, its mole fraction dependence is presented as well.

In Figure 2, the variations of the heats of transfer and the thermal diffusion coefficients for oxygen, hydrogen, and water vapor with the oxygen mole fraction are presented. It shows that the heats of transfer by oxygen and water vapor are positive and those by hydrogen are negative, which means oxygen and water vapor release heat while hydrogen takes up heat during the thermal diffusion. Heats of transfer by each mole component satisfy $Q^*_{\mathrm{O}_2} > Q^*_{\mathrm{H}_2\mathrm{O}} > |Q^*_{\mathrm{H2}}|$. The heats of transfer of oxygen and water vapor decrease with increasing mole fraction, but the absolute value increases in the case of the hydrogen. Approximate linear relations between the heats of transfer and the mole fractions of oxygen hold for the three gases. When linear relations are applied, the maximum deviations are +9% for hydrogen, +4 for oxygen, and +2% for water vapor.

Nonlinear relations exist between the thermal diffusion coefficients and the mole fraction of oxygen under the conditions

TABLE 1: Molar Mass, Diameter, and Thermal Conductivity of the Components

	H_2	O_2	H_2O
M_i (kg/mol)	0.002	0.032	0.018
d_i ($\times 10^{-10}$ m)	1.28	2.92	2.74
λ_i ($\times 10^{-3}$ W/K m)	211.8	32.2	24.2

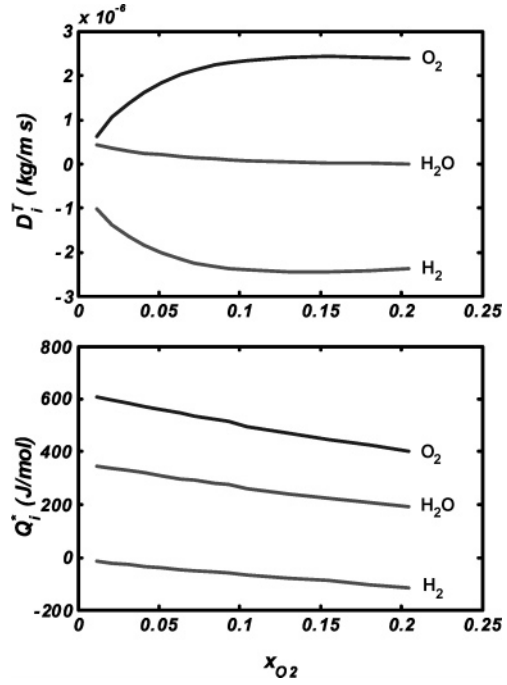

Figure 2. Concentration dependences of heats of transport and thermal diffusion coefficients for O_2, H_2, and H_2O.

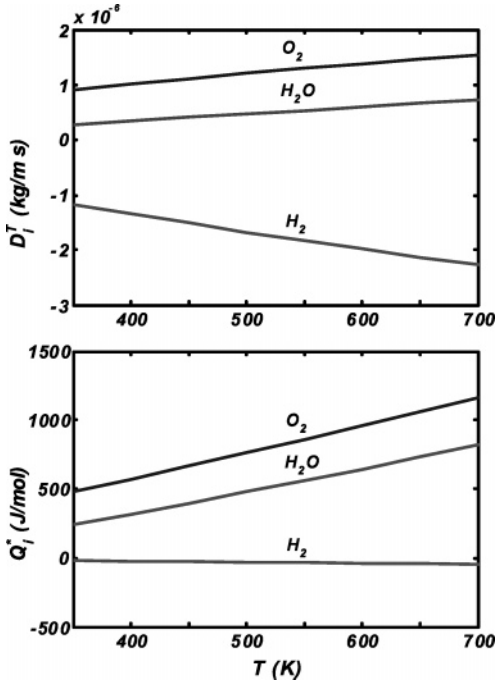

Figure 3. Temperature dependences of the thermal diffusion coefficients and heats of transfer for H_2, O_2, and H_2O.

of our model reactions. The thermal diffusion coefficients are positive for oxygen and negative for hydrogen, which mean that the oxygen thermally diffuses from the hot catalyst surface to the cold gas bulk phase and the hydrogen thermally diffuses to the hot surface. The thermal diffusion coefficients for oxygen and hydrogen increase smoothly with the mole fraction until they reach a maximum at $x_{O_2} \approx 0.15$, then decrease slightly. The water vapor thermally diffuses from the hot catalyst surface to the bulk of the gas phase when the mole fraction of oxygen is less than 0.2, since its thermal diffusion coefficients are positive. When the mole fraction of oxygen is more than 0.2, the thermal diffusion coefficient of water becomes negative, which means water starts thermal diffusion to the hot surface. That results in a lower reaction rate. Therefore, a mole fraction of oxygen less than 0.2 is favorable to the reaction.

An interesting phenomenon is that the heat of transfer by water and its thermal diffusion coefficient decrease with the mole fraction of oxygen even if the mole fraction of water is kept constant. The heat of transfer by one component not only depends on its own concentration but also on the other concentrations, as also follows from eq 4. It demonstrates that in a multicomponent system different components interact with each other, which makes the system more complex than the binary system. The calculated heats of transfer here are comparable to the values obtained by Mill et al.[19] for a liquid mixture (in the work by Mill et al., the definition of the heats of transfer are a factor R different from ours).

At constant mole fractions, for instance, $x_{H_2} = 0.955$, $x_{O_2} = 0.0212$, and $x_{H_2O} = 0.0238$, the heats of transfer and thermal diffusion coefficients are calculated with variation of temperatures from 350 to 700 K and plotted in Figure 3. Approximate linear relations are observed for both the heats of transfer and the thermal diffusion coefficients. If linear relations are used for the heats of transfer, the maximum deviation for the calculations is +2.5%. The maximum deviations from linearity for the thermal diffusion coefficients are about −5.5% for hydrogen and less than 0.5% for oxygen and water. The absolute value of the heats of transfer by each component increases with increasing temperature. The order of magnitude of the heat transported by oxygen is changed in this temperature range. The variation is about 2 J/mol K.

3. Resistivity Coefficients

To use eq 1 to calculate the surface temperature and concentrations, the resistivity coefficients are required. The resistivities are calculated by using the method given by Bedeaux and Kjelstrup.[11] The heat transfer resistivities r_{qq} are related to the thermal conductivity of the gas mixture λ_m as

$$r_{qq} = \frac{\delta}{\lambda_m T^2} \tag{5}$$

where δ is the thickness of the layer. The coupling resistivities are given by

$$r_{qi} = r_{iq} \equiv -r_{qq} Q_i^* \tag{6}$$

The Maxwell−Stefan diffusion coefficients are related to the resistivities by

$$R_{ji} = R_{ij} = r_{ji} - \frac{r_{jq} r_{qi}}{r_{qq}} = -\frac{\delta R}{c D_{ij}} = -\frac{\delta R^2 T}{p D_{ij}} \quad \text{for } i \neq j \tag{7}$$

where the ideal gas law is used and p is total pressure of the gas mixture; see the discussion in the appendix. The diagonal coefficients are obtained by using the relation

$$\sum_{i=1}^{n} c_i R_{ij} = \sum_{i=1}^{n} c_i R_{ji} = 0 \tag{8}$$

The mass transfer resistivities are subsequently calculated by

$$r_{ij} = R_{ij} + \frac{r_{iq} r_{qj}}{r_{qq}} \tag{9}$$

The following calculations are for a catalyst pellet of 2.149 g with a diameter of 1.86 cm. The conditions are taken from

the paper by Maymo et al.[12] The gas mole fractions are 0.857 for H_2, 0.111 for O_2, and 0.032 for H_2O, respectively, with the average temperature 373.6 K and the pressure 1 atm. Under these conditions, the average reaction rate is 140.5×10^{-6} mol/s per gram of catalyst. The thermal conductivities of three gases at temperature of 374 K are taken from ref 28 and are shown in Table 1. The thermal conductivity of the gas mixture is calculated from the relation $\lambda_m = \sum_i x_i \lambda_i$. The thickness of the thin film is chosen here as $\delta = 0.1$ mm. The resulting resistivity matrix in SI units is then given by

$$\begin{pmatrix} r_{qq} & r_{q\mathrm{H}} & r_{qO} & r_{qw} \\ & r_{\mathrm{HH}} & r_{\mathrm{HO}} & r_{\mathrm{H}w} \\ & & r_{\mathrm{OO}} & r_{\mathrm{O}w} \\ & & & r_{ww} \end{pmatrix} =$$

$$\begin{pmatrix} 3.855 \times 10^{-9} & 2.407 \times 10^{-7} & -1.632 \times 10^{-6} & -7.853 \times 10^{-7} \\ & 1.103 \times 10^{-2} & -6.771 \times 10^{-2} & -6.061 \times 10^{-2} \\ & & 6.102 \times 10^{-1} & -3.034 \times 10^{-1} \\ & & & 2.676 \end{pmatrix}$$

and will be used in the following. Since the coefficient matrix obeys Onsager symmetry, only 10 out of 16 values are presented.

4. Surface Temperature and Concentrations

In the steady state, the molar fluxes for the three components comply with the reaction stoichiometric relation and are related to the surface reaction rate as

$$J_{\mathrm{H}_2} = 2J_{\mathrm{O}_2} = -J_{\mathrm{H}_2\mathrm{O}} = \frac{r^s}{A} = J \tag{10}$$

where r^s is the average surface reaction rate and A the external surface area of the catalyst pellet. The direction of the molar flux to the surface is defined as positive.

That temperature and concentration gradients are assumed only to exist in a thin film around the catalyst pellet is somewhat different from the real conditions in the experiment. The assumption is that the solid catalyst has a better heat conduction up to the surface of the pellet. In that case, the surface temperature T^s and the pellet temperature are equal, and presumed equal to the temperature in the gas film near the surface.

The possibility of a temperature profile inside the catalyst is worth some consideration. The conversion may also be active inside the pores of the porous catalyst pellet. The temperature gradient inside the catalyst seems probable for a porous material, in view of the very low thermal conductivity for a solid catalyst, which has been determined experimentally. The measured value of 0.26 W/(K.m) is only marginally higher than the thermal conductivity of the gas mixture itself, which was 0.21 W/(K.m).

Inside such a porous pellet, the net energy is still constant in the steady state. No extra energy will be accumulated in the pellet or at the surface. This is only possible if all the generated energy of the conversion is transported away. The temperature inside a porous catalyst pellet will inevitably be higher than the surface temperature T^s at its external surface if there are catalytic conversion inside the catalyst pores and the low thermal conductivity of the porous material. Some layer of the catalyst material, inward from its external surface, behaves as an extension of the gas film around the catalyst surface. That additional part of the film generates a big percentage of the overall reaction heat. The direction of the net heat fluxes inside the catalyst can only be from inside to the external surface, since all heat generated by reactions inside the pores and at the surface of the catalyst particle must eventually pass through the external surface and into the gas phase. The transfer is, of course, through the gaseous boundary layer, which is part of our idealized film model.

TABLE 2: Surface Temperatures and Mole Fractions by Using Reaction Rate

	measured	calculated		prediction error
		Dufour effect	no Dufour effect	
T^s (K)	390.7	393.3	393.3	0.6%
	given value	Soret effect	no Soret effect	
$x^s_{\mathrm{H}_2}$	0.107	0.8576	0.8559	0.5%
$x^s_{\mathrm{O}_2}$		0.10757	0.10901	
$x^s_{\mathrm{H}_2\mathrm{O}}$		0.0350	0.0352	

Therefore, the following relation holds for the effective fluxes into the medium

$$J_e = J'_q + J_{\mathrm{H}_2}H_{\mathrm{H}_2} + J_{\mathrm{O}_2}H_{\mathrm{O}_2} + J_{\mathrm{H}_2\mathrm{O}}H_{\mathrm{H}_2\mathrm{O}} = J'_q - r^s\Delta_r H/A = 0 \tag{11}$$

The heat flux can be calculated by

$$J'_q = \frac{r^s\Delta_r H}{A} \tag{12}$$

where H_i is the molar enthalpy of component i and $\Delta_r H$ the reaction enthalpy, 244.34 kJ/mol at 374 K. The chemical potential in eq 1 is related to the mole fraction by, assuming ideal gas conditions,

$$\mu_i = \mu_i^0 + RT \ln x_i \tag{13}$$

In our model system, both the reaction rate and the mole fraction of oxygen near the surface were given so that we can use these two parameters to predict the other ones. This allows for two routes to calculate the surface quantities. The first route starts with the reaction rate to calculate the surface temperature and mole fractions near the surface. The second route starts with the concentration near the surface to calculate the others.

First, the measured reaction rate is used to predict the surface temperature and mole fractions. In our model experiment, the gas temperature T^g is 356.6 K. The surface temperature and mole fractions calculated by using eq 1 are listed in Table 2. We conclude that the reaction rate can be used to predict the surface temperature within experimental error. There appears not to be a significant influence of the Dufour effect. At first glance, the mole fractions near the surface, indicated by a superscript s and listed in Table 2, appear to be similar. Also, the influence of the Soret effect appears to be negligible.

However, in view of the temperature and the mole fraction differences across the film, e.g., $\Delta T = 34.1$ K and $\Delta x_{\mathrm{O}} = 0.004$, the relative deviations are quite large. The relative deviation for the calculated surface temperature is then 8%. Considering the Soret effect, the relative deviation for prediction of the oxygen mole fraction near the surface is 14%. This relative deviation is extremely large, 50%, without considering the Soret effect. Hence, we conclude that the prediction for the mole fractions near the surface is unreliable without considering the Soret effect.

The second route starts from the mole fraction near the surface. First, we replace J'_q, J_i, and μ_i in eq 1 with eqs 10, 12,

TABLE 3: Surface Temperature and Reaction Rate by Using Oxygen Surface Mole Fraction

		measured	calculated		
			Dufour & Soret	no Soret	no Dufour
$x^s_{O_2} = 0.107$	T^s (K)	390.7	400.25	440	400.26
	$T^s_{calcd} - T^s_{meas}$ (K)		9.6	49	9.6
	r^s ($\times 10^{-6}$ mol/s g_{cat})	140.5		285.2	164.2
	prediction error for r^s			103%	17%
$x^s_{O_2} = 0.10757$	T^s (K)	390.7	393.31	426	393.32
	$T^s_{calcd} - T^s_{meas.}$ (K)		2.6	35	2.6
	r^s ($\times 10^{-6}$ mol/s g_{cat})	140.5		244.1	140.5
	prediction error for r^s			74%	0%

and 13 and find the following expressions for the molar flux and the surface temperature

$$\begin{cases} J\left(r_{qO}\Delta_r H + r_{OH} + \frac{1}{2}r_{OO} - r_{OW}\right) = R \ln \frac{x^g_O}{x^s_O} \\ \frac{1}{T^s} - \frac{1}{T^g} = J\left(r_{qq}\Delta_r H + r_{qH} + \frac{1}{2}r_{qO} - r_{qW}\right) \end{cases} \quad (14)$$

We find that the surface temperature and the reaction rate are very sensitive to the mole fractions near the surface. In Table 3, this is illustrated by calculating these quantities for two slightly different mole fractions of oxygen near the surface. The value of 0.107 comes from the model system,[12] and the value of 0.107 57 comes from the previous calculations in the first route. Again, the Dufour effect is negligible, and the Soret effect is significant. Considering the Soret effect, the surface temperature and the reaction rate are predicted very well, especially in the case of using the mole fraction of oxygen near the surface from the previous calculations, $x^s_{O_2} = 0.107\,57$. The predicted surface temperature is only 2.6 K different from the measured value, which is within the experimental error. We conclude that the predicted surface temperature and the reaction rate are unreliable when the Soret effect is not considered.

The molar fluxes of oxygen are also calculated for the two mole fractions of oxygen near the surface. We find 0.1624 mol/(m^2 s) and 0.1390 mol/(m^2 s), respectively. Again, a small difference of 0.5% for the mole fractions of oxygen near the surface corresponds to a 14% error in the difference of the mole fractions across the film and induces about 17% deviation in the prediction of the molar flux of oxygen. Therefore, we conclude that the mole fraction near the surface is not known accurately enough to be used for predictions.

In our model reaction, the thermal diffusion effect is found to reduce the reaction rate about 74%, because the thermal diffusion induces the oxygen to thermally diffuse from the reacting surface to the gas bulk phase. Similar results were found by Jenkinson[9] for a chemical vapor deposition reactor that the deposition rate can be lowered or raised to 7−20% because of the multicomponent thermal diffusion. However, how the changed surface reaction rate due to the thermal diffusion influences the surface temperature had not been calculated before. Here, we find that the reduced reaction rate produces a lower surface temperature, because the heat released by the surface reaction is decreased.

5. Discussion

The mole fraction of the water vapor at the entrance of the reactor or the inlet value was 0.023 in the experiments.[12] We used this value for the mole fraction of water in the gas phase. In the steady state, the mole fraction of water in the gas phase, which was not measured, will be higher than the inlet value. To assess the importance of this, various values were tried to test the influence on the surface temperature and the surface concentrations. With the varying water vapor mole fractions, the resistivities vary as well. The effect of the variation of the water vapor mole fraction is shown in Figure 4. The variations for the various predictions vary linearly with the water vapor mole fraction and are smaller than the error in our calculated values. An interesting observation is that the mole fraction of hydrogen near the surface is about 0.1% higher than in the gas bulk phase, although the hydrogen is consumed by the surface reaction. The reason is that the hydrogen thermally diffuses to the surface, and the thermal diffusion rate is larger than the consumption rate by the surface reaction. We conclude that the choice of the water vapor mole fraction does not influence the reliability of the calculated surface temperature and mole fractions near the surface.

The basis of the film model[29] is the assumption that the resistance to transfer lies in a hypothetical layer next to the interface, where the transfer mechanism is molecular diffusion. The film thicknesses for mass transfer and heat transfer are usually assumed to be slightly different,[29] and a symmetric matrix of δ's could be used in our case. However, in the present case, we find that the use of one film thickness is sufficient. Inside this film, there are temperature and concentration gradients due to the surface reaction. Outside this film, the fluid is assumed to be a homogeneous bulk phase.

Around the range of possible film thickness given by Taylor and Krishna,[21] $\delta = 0.1-1$ mm, we calculated the surface temperature and the mole fraction of oxygen near the surface; see Figure 5. The calculated surface temperature and mole fraction of oxygen near the surface vary linearly with film thickness. When the film thickness is chosen as 0.0935 mm, the calculated surface temperature is exactly the same as the measured surface temperature, 390.7 K, but the calculated mole fraction of oxygen near the surface is much larger than the

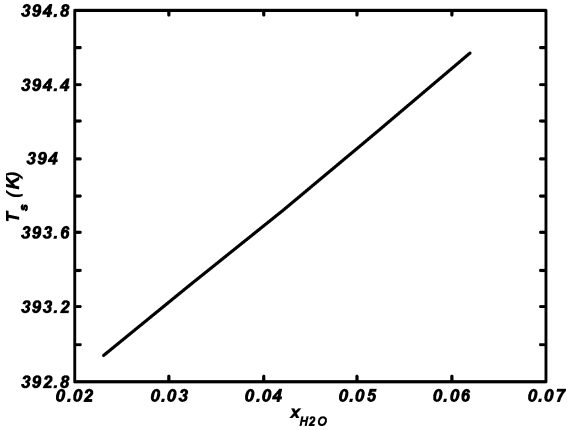

Figure 4. Surface temperature dependence on the water mole fraction keeping x_{O_2} constant in the bulk gas phase.

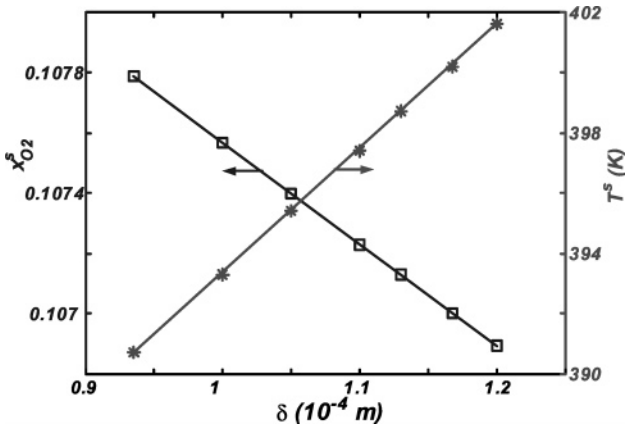

Figure 5. Calculated surface temperature and surface mole fraction of oxygen when various thickness of the thin film is chosen.

measured value. If the film thickness is increased up to 0.120 mm, the calculated surface temperature is 401.6 K, which is not so close to the measured value any more. On the other hand, the calculated mole fraction of oxygen near the surface is exactly the same as the one given in the model system in the case of $\delta = 0.1168$ mm. However, the corresponding surface temperature is 400.2 K, which is much higher than the measured value. On the basis of these calculations, the film thickness is determined in the range 0.0935−0.1168 mm. In the above calculations, the film thickness of 0.1 mm is chosen such that the calculated surface temperature and mole fraction are close to the values given in our model system. The film thickness is a sensitive parameter for the predictions.

6. Effective Conductivity Coefficients

A second set of flux−force equations was proposed to predict the surface temperature and mole fractions as described by eq 2. It involved the effective conductivity coefficients $l_{i,\mathrm{eff}}$. To investigate the validity of this method, the same model reaction[12] is used, and similar calculations are repeated. The results are compared to the previous values calculated by using the resistivities.

To find the expressions for the *l*-coefficients, a similar procedure as for the resistivities is used. When Fick's effective diffusion coefficient $D_{i,\mathrm{eff}}$ is used, the flux−force equation is written as[21]

$$J_i = -D_{i,\mathrm{eff}} \frac{\mathrm{d}c_i}{\mathrm{d}x} \tag{15}$$

Substituting the chemical potential μ_i in eq 2 with the relation

$$\mu_i = \mu_i^\circ + RT \ln \frac{c_i}{c} \tag{16}$$

using the ideal gas law and comparing eq 2 and the integral of eq 15, one obtains

$$l_{i,\mathrm{eff}} = \frac{x_i D_{i,\mathrm{eff}} p}{\delta R^2 T} \tag{17}$$

The Fick's effective diffusion coefficient is calculated by[21,30]

$$\frac{1}{D_{i,\mathrm{eff}}} = \sum_{\substack{j=1 \\ j\neq \mathrm{i}}}^{n} \frac{x_j}{D_{ij}} \left(1 - \frac{x_i J_j}{x_j J_i}\right) \tag{18}$$

For a surface reaction, the flux ratios J_j/J_i are constant in the thin film and related to the ratios of stoichiometric coefficients of the chemical reaction. In fact, this is why this description is so useful here. The conductivity heat transfer coefficient l_{qq} is calculated by

$$l_{qq} = \frac{\lambda_m T^2}{\delta} \tag{19}$$

This relation can be obtained by comparing eq 2 to the Fourier's law.

The coupling conductivity coefficients are related to the heats of transfer in the following derivation. When the temperature difference is zero, eq 2 become

$$\begin{cases} J'_q = -\dfrac{1}{T}\displaystyle\sum_i l_{qi} \Delta\mu_{i,T}|_{\Delta T=0} \\ J_i = -\dfrac{1}{T} l_{i,\mathrm{eff}} \Delta\mu_{i,T|\Delta T=0} \end{cases} \tag{20}$$

Comparing these two equations, one obtains

$$(J'_q)_{\Delta T=0} = \sum_i \frac{l_{qi}}{l_{i,\mathrm{eff}}} (J_i)_{\Delta T=0} \tag{21}$$

When the temperature difference in the thin film is zero, the heat flux due to the molar flux is also written as

$$(J'_q)_{\Delta T=0} = \sum_i Q_i^* (J_i)_{\Delta T=0} \tag{22}$$

where Q_i^* is also the heat of transfer carried by the component *i*. Comparing eq 21 to 22, the heat of transfer Q_i^* is

$$Q_i^* = \frac{l_{qi}}{l_{i,\mathrm{eff}}} \tag{23}$$

which is similar to the definition given by Kjelstrup and Bedeaux[25] for a binary component system.

When the molar flux of the component *i* vanishes, namely, $J_i = 0$, which means that the chemical potential difference is caused only by the thermal diffusion, the lower equation in eq 2 is rewritten as

$$l_{qi} \Delta\left(\frac{1}{T}\right) = \frac{1}{T} l_{i,\mathrm{eff}} \Delta\mu_{iT}|_{J_i=0} \tag{24}$$

Replacing l_{qi} with eq 23 and rewriting eq 24, one obtains

$$\Delta\mu_{i,T} = -Q_i^* \frac{\Delta T}{T}\bigg|_{J_i=0} \tag{25}$$

Comparing eq 25 to eq 31 in the Appendix, one obtains the same expression as eq 3 for the heat of transfer.

Fick's effective diffusion coefficients of the three gas components are calculated by using eq 18 in SI units for $T = 373.6$ K, $x_{\mathrm{H_2}} = 0.857$, $x_{\mathrm{O_2}} = 0.111$, and $x_{\mathrm{H_2O}} = 0.032$. The values are

$$(D_{\mathrm{H,eff}}\ D_{\mathrm{O,eff}}\ D_{W,\mathrm{eff}}) = (7.872 \times 10^{-4}\ 2.123 \times 10^{-4}\ 2.758 \times 10^{-4})$$

The phenomenological *l*-coefficients are calculated by using eqs 17, 19, and 23

$$\begin{pmatrix} l_{qq} & l_{qH} & l_{qO} & l_{qW} \\ & l_{H,eff} & 0 & 0 \\ & & l_{O,eff} & 0 \\ & & & l_{W,eff} \end{pmatrix} =$$

$$\begin{pmatrix} 2.594 \times 10^{8} & -1.653 \times 10^{3} & 3.915 \times 10^{2} & 7.054 \times 10^{1} \\ & 2.647 \times 10^{1} & 0 & 0 \\ & & 9.244 \times 10^{-1} & 0 \\ & & & 3.463 \times 10^{-1} \end{pmatrix}$$

which are used for the following calculations.

Rewriting the flux−force equations using the relation of $\mu_i = \mu_i^0 + RT \ln x_i$, one obtained

$$\begin{cases} J_q' = l_{qq}\left(\dfrac{1}{T^s} - \dfrac{1}{T^g}\right) - R\sum_i l_{qi} \ln\dfrac{x_i^s}{x_i^g} \\ J_i = l_{qi}\left(\dfrac{1}{T^s} - \dfrac{1}{T^g}\right) - R\, l_{i,eff} \ln\dfrac{x_i^s}{x_i^g} \end{cases} \tag{26}$$

which are used to repeat the calculations for the surface quantities. The results are almost the same as in the first method. The maximum deviation from the previous results is about 0.01%. We conclude that the effective conductivity coefficients are efficient to be used for the calculations. The reason is that the effective *l*-coefficients for the mass transfer include the contribution from the coupling between various components. The previously used Kubota method[21,30] of effective diffusion coefficients is indeed appropriate to calculate the Fick's effective diffusion coefficients in a stagnant gas film for catalytic reactions. Heats of transfer can be defined in two ways by using the resistivity for heat transfer and the effective conductivity coefficients for mass transfer, respectively. Both methods are working very well.

7. Conclusions

We have demonstrated that TIP can be used to predict surface temperature and concentrations for catalytic hydrogen oxidation reaction with reasonable accuracy. TIP is chosen because it allows for a systematic way to comprise coupling between heat and mass transfer. Two reciprocal methods have been used that yield the same results and fit the experimental data very well. In the second simplified method, the effective *l*-coefficients for mass transfer are proven to work efficiently. Two definitions for the heats of transfer in terms of the ratio of resistivity or conductivity coefficients are possible, and both yield essentially the same results.

The oxygen is found to have the largest heat of transfer among the three gases. The heats of transfer change approximately linearly with the mole fractions and the temperature. In contrast, the thermal diffusion coefficients, the most important parameter of the coupling effect, change nonlinearly with the mole fractions but almost linearly with temperature. An interesting observation is that the mole fraction of hydrogen near the surface is about 0.1% higher than that in the gas bulk phase, although hydrogen is consumed by the surface reaction. The reason is that the hydrogen thermally diffuses to the catalyst surface, and the diffusion rate is large in comparison to the consumption rate by the surface reaction.

The reaction rate can be used to predict the surface temperature and the surface concentrations. The mole fraction of oxygen near the surface is not known accurately enough to be used for these predictions. The Dufour effect is found to be negligible for the calculation of the catalyst surface temperature. However, the Soret effect considerably influences the prediction for the mole fractions near the surface.

This is the first time the Soret effect is found to significantly influence the surface temperature. The calculated surface temperature difference by taking into account the Soret effect or not is about 39 K when the mole fraction of oxygen near the surface given in the model system is used. The reason is that the Soret effect resists thermal diffusion of oxygen to the catalyst surface, so the reaction rate and consequently the catalyst surface temperature are decreased significantly. By considering the Soret effect, the predictions for the surface temperature and the reaction rate work very well.

In comparison to the generally accepted film thickness, a much narrower range is determined by using two known parameters, the surface temperature and concentration. The film thickness is found in the range 0.09−0.12 mm.

Acknowledgment. The authors would like to thank Professor Gert Frens for suggesting the work and Professor Signe Kjelstrup and Dr. Xiaoding Xu for helpful discussions. Professor C. R. Klein is gratefully acknowledged for the program to calculate the coefficient D_i^T.

Appendix

In this Appendix, we shall present two methods to find the expression for the heats of transfer Q_i^*. In the first method, one starts with the Maxwell−Stefan equations[31] for the isothermal mass transfer of a multicomponent mixture

$$\Delta\mu_{i,T} = -RT \sum_{\substack{j=1 \\ j\neq i}}^{n} \frac{x_j(u_i - u_j)}{D_{ij}} \quad i = 1, 2, ..., n \tag{27}$$

in which $u_i \equiv J_i/c_i$ is the velocity of the diffusing component *i*. When large temperature gradients exist, the thermal diffusion contribution to the molar fluxes should be taken into account. Equation 27 can then be augmented[31,32] as

$$\Delta\mu_{i,T} = -RT \sum_{\substack{j=1 \\ j\neq i}}^{n} \frac{x_j(u_i^T - u_j^T)}{D_{ij}} \quad i = 1, 2, ..., n \tag{28}$$

where u_i^T is the augmented species velocity including the contribution due to the thermal diffusion, which is defined[31] as

$$u_i^T = u_i + \left(\frac{D_i^T}{\rho_i}\right)\frac{\Delta T}{T} \quad i = 1, 2, ..., n \tag{29}$$

The thermal diffusion coefficients D_i^T have been defined in the manner of Hirschfelder et al.[27] $\rho_i \equiv c_i M_i$ is the mass density of the component *i*. c_i and M_i are the concentration and the molar mass of the gas component *i*. When only the thermal diffusion contributes to the species velocity

$$u_i^T = \left(\frac{D_i^T}{\rho_i}\right)\frac{\Delta T}{T} \quad i = 1, 2, ..., n \tag{30}$$

Replacing u_i^T in eq 28 with eq 30, the chemical potential difference due to the thermal diffusion is

$$\Delta\mu_{i,\mathrm{T}} = -\sum_{\substack{j=1\\ j\neq i}}^{n} \frac{x_j R\Delta T}{D_{ij}}\left(\frac{D_i^{\mathrm{T}}}{\rho_i} - \frac{D_j^{\mathrm{T}}}{\rho_j}\right) \quad i = 1, 2, ..., n \quad (31)$$

On the other hand, when the temperature difference is zero, the upper equation in eq 1 becomes

$$J_q' = -\sum_{i=1}^{n} \frac{r_{qi}}{r_{qq}} J_i \quad (32)$$

The heat flux due to the molar flux can also be written by

$$J_q' = \sum_{i=1}^{n} Q_i^* J_i \quad (33)$$

where Q_i^* is the heats of transfer by the component *i*. Comparing eq 32 to 33, one obtains

$$Q_i^* = -\frac{r_{qi}}{r_{qq}} \quad (34)$$

which is the same definition as in ref 11. Rewriting the lower equation in eq 1 by using the upper equation in it and eq 34, one has

$$-\frac{\Delta\mu_{i,\mathrm{T}}}{T} = -Q_i^*\Delta\left(\frac{1}{T}\right) + \sum_{j=1}^{n}\left(r_{ji} - \frac{r_{jq}r_{qi}}{r_{qq}}\right)J_j \quad (35)$$

The chemical potential difference caused by the thermal diffusion is then

$$\Delta\mu_{i,\mathrm{T}} = -Q_i^*\frac{\Delta T}{T} \quad (36)$$

Comparing eqs 31 to 36, one obtains

$$Q_i^* = \sum_{j=1}^{n} \frac{x_j RT}{D_{ij}}\left(\frac{D_i^{\mathrm{T}}}{\rho_i} - \frac{D_j^{\mathrm{T}}}{\rho_j}\right) \quad (37)$$

In the second method, we start with eq 35. By using eq 7, eq 35 becomes

$$-\frac{\Delta\mu_{i,\mathrm{T}}}{T} = -Q_i^*\Delta\left(\frac{1}{T}\right) + \sum_{j=1}^{n} R_{ij}J_j \quad (38)$$

When $\Delta\mu_{i,\mathrm{T}}$ is equal to zero, one has

$$-Q_i^*\Delta\left(\frac{1}{T}\right) + \sum_{j=1}^{n} R_{ij}J_j = 0 \quad (39)$$

and eq 2 becomes

$$J_i = l_{qi}\Delta\left(\frac{1}{T}\right) \quad (40)$$

Replacing J_i in eq 39 with eq 40, one obtains

$$Q_i^* = l_{qi}\sum_{j=1}^{n} R_{ij} \quad (41)$$

Replacing R_{ij} in eq 41 with eq 7 and using eq 8, one obtains

$$Q_i^* = \sum_{j=1}^{n} \frac{c_j R\delta}{cD_{ij}}\left(\frac{l_{qj}}{c_j} - \frac{l_{qi}}{c_i}\right) \quad (42)$$

The molar flux due to the thermal diffusion can be also written as

$$J_i^{\mathrm{T}} = u_i^{\mathrm{T}} c_i \quad (43)$$

Substituting u_i^{T} with eq 30 and c_i with relation of $\rho_i \equiv c_i M_i$, eq 43 becomes

$$J_i^{\mathrm{T}} = \left(\frac{D_i^{\mathrm{T}}}{M_i}\right)\frac{\Delta T}{T\delta} \quad (44)$$

Comparing eqs 44 and 40, one has

$$l_{qi} = -\frac{TD_i^{\mathrm{T}}}{\delta M_i} \quad (45)$$

Replacing l_{qi} and c_i in eq 42 with eq 45 and $\rho_i \equiv c_i M_i$, one obtains

$$Q_i^* = \sum_{j=1}^{n} \frac{x_j RT}{D_{ij}}\left(\frac{D_i^{\mathrm{T}}}{\rho_i} - \frac{D_j^{\mathrm{T}}}{\rho_j}\right) \quad (46)$$

The Maxwell−Stefan diffusion coefficient is calculated by[33]

$$D_{i,j} = \sqrt{\frac{2}{\pi^3}}\frac{(RT)^{3/2}}{N_{\mathrm{A}} p d_{i,j}^{\ 2}}\left(\frac{1}{M_i} + \frac{1}{M_j}\right)^{1/2} \quad d_{i,j} = \frac{d_i + d_j}{2} \quad (47)$$

where N_{A} is the Avogadro constant, *p* the total pressure of the gas mixture, and d_i the diameter of the gas molecule *i*.

We note that the two conditions used above are basically the same, namely, only the thermal diffusion causes the molar flux or the chemical potential gradient.

Notation

A external surface area of a catalyst pellet, m^2
c_i molar concentration, mol/m^3
$D_{i,\mathrm{eff}}$ Fick's effective diffusion coefficient of the component *i*, m^2/s
D_i^{T} thermal diffusion coefficient of the component *i*, kg/(m s)
D_{ij} Maxwell−Stefan diffusion coefficient, m^2/s
d diameter of the molecule, m
d_{c} diameter of the catalyst pellet, m
H_i Molar enthalpy of the component *i*, J/mol
J molar flux, and $J = r^{\mathrm{s}}/A$, mol/(m^2 s)
J_i molar flux of the component *i*, mol/(m^2 s)
J_i^{T} molar flux due to the thermal diffusion for component *i*, mol/(m^2 s)
J_q' measurable heat flux, J/(m^2 s)
$l_{i,\mathrm{eff}}$ effective conductivity coefficient for mass transfer, mol^2 K/(J m s)
l_{qi} coupling conductivity coefficient, mol K/(m s)
l_{qq} conductivity coefficient for heat transfer, J K/(m s)
M molar mass, kg/mol
N_{A} Avogadro constant, 6.02×10^{23} mol^{-1}
p total pressure of the gas mixture, Pa
p_i partial pressure of component *i*, Pa
Q_i^* heat transported by component *i* in coupling processes, J/mol

R gas constant, J/(mol K)

R_{ij} resistivities for mass transfer at a constant temperature, J m^2 s/(mol^2 K)

r^s reaction rate, mol/(s $g_{cat.}$)

r_{ij} mass transfer resistivity, J m^2 s/(mol^2 K)

r_{qi} coupling resistivity, m^2 s/(mol K)

r_{qq} heat transfer resistivity, m^2 s/(J K)

T temperature, K

T^s temperature at the catalyst surface, K

T^g temperature in the bulk of gas phase, K

u_i velocity of the diffusing component i, m/s

u_i^T augmented species velocity including the contribution due to the thermal diffusion, m/s

x_i mole fraction of the component i, dimensionless

x_i^s mole fraction near the catalyst surface, dimensionless

x_i^g mole fraction in the bulk of gas phase, dimensionless

Greek Letters

λ_i thermal conductivity of the component i, mW/(m K)

λ_m thermal conductivity of the gas mixture, mW/(m K)

ρ_i density of the component i, kg/m^3

δ thickness of the gas film, m

μ_i chemical potential of component i, J/mol

μ_i^0 chemical potential of component i at standard state, J/mol

$\mu_{i,T}$ chemical potential of component i at constant temperature, J/mol

Δ differences across the gas film

$\Delta_r H$ reaction enthalpy, kJ/mol

References and Notes

(1) Sawford, B. L.; Spurling, T. H.; Thurley, D. S. The diffusion thermoeffect (Dufour effect) in gaseous mixtures of hydrogen and carbon dioxide. *Aust. J. Chem.* **1970**, *23*, 1311−1320.

(2) Hort, W.; Linz, S. J.; Lucke, M. Onset of convection in binary gas mixtures: Role of the Dufour effect. *Phys. Rev. A* **1992**, *45* (6), 3737−3748.

(3) Linz, S. J. Binary mixtures: Onset of Dufour driven convection. *Phys. Rev. A* **1989**, *40* (12), 7175−7181.

(4) Boushehri, A.; Abbaspour, A. Diffusion thermoeffect in gases (the Dufour effect). *Bull. Chem. Soc. Jpn.* **1979**, *52* (7), 2097−2098.

(5) Rastogi, R. P.; Madan, G. L. Cross-phenomenological coefficients, Part 6-Dufour effect in gases. *Trans. Faraday Soc.* **1966**, *62*, 3325−3330.

(6) Lhost, O.; Platten, J. K. Large-scale convection induced by the Soret effect. *Phys. Rev. A* **1989**, *40* (11), 6415−6420.

(7) Hao, L.; Leaist, D. G. Large Soret effect for silicotungstic acid in a supporting electrolyte-9-percent change in concentration per degree. *J. Phys. Chem.* **1994**, *98* (51), 13741−13744.

(8) Liu, J.; Ahlers, G. Rayleigh-Benard convection in binary-gas mixtures: Thermophysical properties and the onset of convection. *Phys. Rev. E* **1997**, *55* (6), 6950−6968.

(9) Jenkinson, J. P.; Pollard, R. Thermal diffusion effects in chemical vapor deposition reactors. *J. Electrochem. Soc.* **1984**, *131* (12), 2911−2917.

(10) Leakeas, C. L.; Sharif, M. A. R. Effects of thermal diffusion and substrate temperature on silicon deposition in an impinging-jet CVD reactor. *Numer. Heat Transfer, Part A* **2003**, *44* (2), 127−147.

(11) Bedeaux, D.; Kjelstrup, S. Irreversible thermodynamics--a tool to describe phase transitions far from global equilibrium. *Chem. Eng. Sci.* **2004**, *59*, 109−118.

(12) Maymo, J. A.; Smith, J. M. Catalytic oxidation of hydrogen-Intropellet heat and mass transfer. *AIChE J.* **1966**, *12* (5), 845−854.

(13) Bearman, R. J.; Horne, F. H. Comparison of theories of heat of transport and thermal diffusion with experiments on cyclohexane-carbon tetrachloride system. *J. Chem. Phys.* **1965**, *42* (6), 2015.

(14) Sugisaki, M. Soret coefficients and heat of transport of polyvalent electrolytes in an aqueous solution. *Bull. Chem. Soc. Jpn.* **1975**, *48* (10), 2751−2754.

(15) Demichowiczpigoniowa, J. Temperature and concentration dependence of soret coefficient for aqueous copper-sulfate solutions. 1. Soret coefficient and heat of transport at 25 degrees. *Electrochim. Acta* **1977**, *22* (9), 1031−1033.

(16) Rowley, R. L.; Horne, F. H. Dufour effect. 3. Direct experimental determination of the heat of transport of carbon tetrachloride-cyclohexane liquid mixtures. *J. Chem. Phys.* **1980**, *72* (1), 131−139.

(17) Rowley, R. L.; Yi, S. C.; Gubler, V.; Stoker, J. M. Mutul diffusivity, thermal conductivity and heat of transport in binary liquid mixtures of alkanes in carbon tetrachloride. *Fluid Phase Equilib.* **1987**, *36*, 219−233.

(18) Allnatt, A. R. Corrected expression for the heat of transport. *Mol. Phys.* **1994**, *82* (4), 781−785.

(19) Clinton, T. M.; David, L. B.; Piergiorgio, C.; Leon, F. P. Onsager heat of transport measured at the n-heptanol liquid-vapor interface. *J. Phys. Chem. B* **2004**, *108*, 2681−2685.

(20) Rudakov, V. I.; Ovcharov, V. V. Mathematical description of the diffusion in a temperature field and measuring the heat of transport. *Int. J. Heat Mass Transfer* **2002**, *45*, 743−753.

(21) Taylor, R.; Krishna, R. *Multicomponent mass transfer*; Wiley: New York, 1993; Chapter 8.

(22) Palle, S.; Nolan, C.; Miller, R. S. On molecular transport effects in real gas laminar diffusion flames at large pressure. *Phys. Fluids* **2005**, *17* (10), 103601.

(23) Bongers, H.; De Goey, L. P. H. The effect of simplified transport modeling on the burning velocity of laminar premixed flames. *Combust. Sci. Technol.* **2003**, *175* (10), 1915−1928.

(24) Rosner, D. E.; Israel, R. S.; La Mantia, B. 'Heavy' species Ludwig-Soret transport effects in air-breathing combustion. *Combust. Flame* **2000**, *123* (4), 547−560.

(25) Kjelstrup, S.; Bedeaux, D. *Elements of irreversible thermodynamics for engineers*. International Center for Applied Thermodynamics, Istanbul, 2001.

(26) Kleijn, C. R. Chemical vapor deposition processes. In *Computational modeling in semiconductor processing*; Meyyappan, M., Ed.; Artech House: Boston, 1995; Chapter 4, pp 97−229.

(27) Hirschfelder, J. O.; Curtiss, C. F.; Bird, R. B. *Molecular theory of gases and liquids*, 4th ed.; Wiley: New York, 1967; Chapters 7, 8.

(28) Touloukian, Y. S. Thermal conductivity, nonmetallic liquids and gases. In *Thermophysical properties of matter*; IFI/Plenum Press: New York, 1970; Vol. 3.

(29) Coulson, J. M.; Richardson, J. F.; Backhurst, J. R.; Harker, J. H. *Chemical engineering—Fluid flow, heat transfer and mass transfer*, 4th ed.; Pergamon Press: Oxford, 1993; Vol. 1, Chapters 10, 11.

(30) Kubota, H.; Yamanaka, Y.; Dalla Lana, I. G. Effective Diffusivity of multicomponent gaseous reaction system. *J. Chem. Eng. Jpn.* **1969**, *2*, 71−75.

(31) Krishna, R.; Wesselingh, J. A. The Maxwell-Stefan approach to mass transfer. *Chem. Eng. Sci.* **1997**, *52* (6), 861−911 (review article no. 50).

(32) Kuiken, G. D. C. *Thermodynamics of irreversible processes: Applications to diffusion and rheology*; Wiley: Chichester, U.K., 1994.

(33) Wesselingh, J. A.; Krishna, R. *Mass transfer in multicomponent mixtures*; Delft University Press: Delft, The Netherlands, 2000; p 95.